Journal of Physics: Conference Series **2919** (2024) 012028 doi:10.1088/1742-6596/2919/1/012028

Kerr-Quintic Nonlinearities in Graphene Quantum Dot

Abhijit Shayam[1]*, Monika Nath[1], Rohit Mukherjee[2], Nitu Borgohain[1]

[1]Department of Physics, University of Science & Technology Meghalaya (USTM), Meghalaya, India-783101
[2]Theoretical Photonics Group, Department of Physics, Sarala Birla University, Jharkhand, India-835103

Corresponding Author: abhijit.shyam12@gmail.com

Abstract: This paper deals with the higher-order nonlinearities in graphene quantum dots as defect layer in one dimensional photonic crystal. A weak probe pulse and two strong control laser beams are employed in a close loop ladder type configuration under an electromagnetically induced transparency regime. In the system, the existence of third- and fifth-order susceptibilities are found to be as large as $\sim 10^{-15} m^2/V^2$, and $\sim 10^{-27} m^4/V^4$, respectively, at the probe wavelength 1.55 μm. The systems possessing such large nonlinearities can be employed to fabricate nonlinear optical devices, operable at much low power level.

Key words: One Dimensional Photonic crystal, Graphene Quantum Dot, Kerr-Quintic susceptibilities, Electromagnetically Induced Transparency.

1. Introduction

The nonlinear light-matter interactions in atomic systems, quantum wells and quantum dots have attracted a lot of attention in recent years, both theoretically and experimentally [1-3]. Solid-state devices utilizing both interband and inter-subband transitions in quantum dots offer intrinsic advantages over atomic gas counterparts, such as large electric dipole moments and high nonlinear coefficients, these intrinsic properties offers the optical materials to fabricate highly sensitive optical systems operable at much lower power [1-6]. Quantum dots offer extensive design flexibility for devices. They can be tailored to have different transition energies, dipole moments, and symmetries based on the chosen material. Additionally, they can be easily integrated with other semiconductor devices [7, 8].

One of the most effective techniques to enhance nonlinear optical properties in QDs is electromagnetically induced transparency (EIT). EIT is a quantum interference effect that provides a usually translucent medium transparent to the probe light under the influence of a control light, effectively minimizing absorption and augmenting nonlinear properties [8-10]. EIT has been extensively studied for its ability to enhance nonlinear optical processes by reducing the absorption of the probe light. Recent studies have extended EIT to QD systems, demonstrating significant enhancements in nonlinear optical properties. For instance, Zhang et al. [11] showed that EIT in QD

Content from this work may be used under the terms of the Creative Commons Attribution 4.0 licence. Any further distribution of this work must maintain attribution to the author(s) and the title of the work, journal citation and DOI.
Published under licence by IOP Publishing Ltd

systems could lead to large third-order or Kerr nonlinearities, making them suitable for low-power photonic applications, while Hachim et al. [12] reported to slow down the light in a double quantum dot system by three orders, while enhancing the susceptibility by two order. In addition, Xu and Malko [13] demonstrated large third-order nonlinear optical coefficients in semiconductor QDs, highlighting their potential in optical switching and modulation applications. Similarly, Klimov [14] reported on the enhanced nonlinear optical responses in colloidal quantum dots, attributing the effects to quantum confinement and surface states. EIT has been also employed to investigate its ability to enhance fifth-order or quintic nonlinearity in the semiconductor QDs, for example, Liu et al. [15] explored the quintic nonlinearity under EIT in QDs, revealing enhanced fifth-order susceptibilities and potential for ultrafast optical switching. Research by Kang *et al.* [16] showed substantial quintic nonlinearity in semiconductor QDs, suggesting potential applications in ultrafast optical processes. Further studies by Chen *et al.* [17] indicated that quintic nonlinear effects could be crucial for understanding the full nonlinear response in QD systems under high-intensity fields. Based on the above literature, it is clear that the enhancement of nonlinear optical properties in QDs is very crucial from the point of view of effective applications. Thus, we aim in this article to explore and quantify the Kerr and quintic nonlinearities in QD systems under EIT, contributing to the advancement of nonlinear photonic devices operating at low power levels.

The paper has been laid out in the following way: in Section 2, the three-level GQD theoretical model that interacts with the optical fields is presented, followed by the evaluation of the linear and nonlinear susceptibilities. Section 3 delves into exploring the properties of susceptibilities under varied control field parameters. Lastly, Section 4 encapsulates a concise summary and conclusion.

2. Mathematical Model and Governing Equations

For this study, we chose a nitrogen-doped graphene quantum dot (GQD). These GQDs are integrated as an ensemble within the defect layer of a one-dimensional photonic crystal (1DPC) [18]. GQDs operate as three-level quantum systems and are controlled by three coherent laser fields. The proposed layered medium is a one-dimensional photonic crystal (1DPC) featuring a centrally embedded defect layer doped with Graphene Quantum Dots (GQDs). The materials used are SiO_2 with a refractive index of $n_{SiO_2} = 1.47$ and TiO_2 with a refractive index of $n_{TiO_2} = 2.28$ [18]. Here we took the central wavelength as a probe wavelength for the doped GQD system ($\lambda_0 \approx \lambda_p 1.55\ \mu m$).

In the ladder-type configuration of GQDs, the three energy states are designated as the lower level $|1\rangle$, the intermediate level $|2\rangle$, and the upper level $|3\rangle$. A weak probe field with an angular frequency ω_p, amplitude E_p and Rabi-frequency $\Omega_p = \frac{\mu_{21}E_p}{2\hbar}$ is coupled to the $|1\rangle \rightarrow |2\rangle$ transition, while a first strong control field with an angular frequency ω_d amplitude E_d and Rabi-frequency $\Omega_d = \frac{\mu_{32}E_d}{2\hbar}$ is coupled to the $|2\rangle \rightarrow |3\rangle$ transition and a second control field with an angular frequency ω_c amplitude E_c and Rabi-frequency $\Omega_c = \frac{\mu_{31}E_c}{2\hbar}$ is coupled to the $|1\rangle \rightarrow |3\rangle$ transitions depicted in Fig. 1. Here, μ_{ij} are the

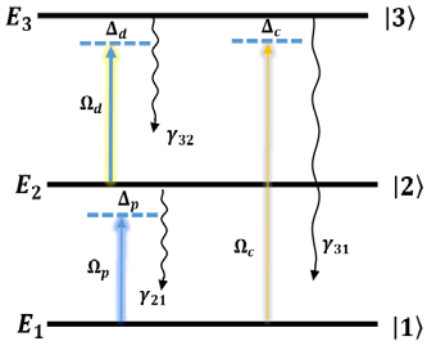

Fig-1: Schematic of energy levels graphene quantum dot with close loop ladder type transition.

corresponding electric dipole moments. The applied electric fields in the GQD system is

$$\vec{E} = \hat{e}_p E_p e^{-i\omega_p t} + \hat{e}_d E_d e^{-i\omega_d t} + \hat{e}_c E_c e^{-i\omega_c t} + c.c., \tag{1}$$

In the equation (1),$\hat{e}_p$,$\hat{e}_d$, $\hat{e}_c$ are unit vectors of along the polarization direction of the respective electric fields. In the Schrödinger picture, the semi-classical Hamiltonian for the GQDs system can be expressed as follows:

$$\hat{H} = \sum_{i=1}^{3} \hbar\omega_i |i\rangle\langle i| - \hbar\left(\Omega_p e^{-i\omega_p t}|1\rangle\langle 2| + \Omega_d e^{-i\omega_d t}|2\rangle\langle 3| + \Omega_c e^{-i\omega_c t}|1\rangle\langle 3| + h.c.\right), \tag{2}$$

where, $\hbar\omega_i$ is the energy associate with the state $|i\rangle$ of the GQD, $|i\rangle\langle j|$ and $h.c.$ is the Hermitian conjugate. Applying the rotating wave approximation we obtain the Maxwell-Bloch equations,

$$\frac{\partial}{\partial t}\tilde{\rho}_{11} = i\left(\Omega_p{}^*\tilde{\rho}_{12} - \Omega_p\tilde{\rho}_{21}\right) + i(\Omega_c{}^*\tilde{\rho}_{13} - \Omega_c\tilde{\rho}_{31}), \tag{3}$$

$$\frac{\partial}{\partial t}\tilde{\rho}_{22} = -\gamma_2\tilde{\rho}_{22} + i\left(\Omega_p{}^*\tilde{\rho}_{12} - \Omega_p\tilde{\rho}_{21}\right) + i(\Omega_d{}^*\tilde{\rho}_{23} - \Omega_d\tilde{\rho}_{32}), \tag{4}$$

$$\frac{\partial}{\partial t}\tilde{\rho}_{33} = -\gamma_3\tilde{\rho}_{33} + i(\Omega_c{}^*\tilde{\rho}_{13} - \Omega_c\tilde{\rho}_{31}) + i(\Omega_d{}^*\tilde{\rho}_{23} - \Omega_d\tilde{\rho}_{32}), \tag{5}$$

$$\frac{\partial}{\partial t}\tilde{\rho}_{21} = i\left(\Delta_p + \frac{i\gamma_{21}}{2}\right)\tilde{\rho}_{21} + \left\{i\Omega_p(\tilde{\rho}_{11} - \tilde{\rho}_{22}) - i\Omega_c\tilde{\rho}_{23} + i\Omega_d{}^*\tilde{\rho}_{31}\right\}, \tag{6}$$

$$\frac{\partial}{\partial t}\tilde{\rho}_{31} = i\left(\Delta_c + i\frac{\gamma_{31}}{2}\right)\tilde{\rho}_{31} + \left\{i\Omega_c(\tilde{\rho}_{11} - \tilde{\rho}_{33}) - i\Omega_d\tilde{\rho}_{21} + i\Omega_p{}^*\tilde{\rho}_{32}\right\}, \tag{7}$$

$$\frac{\partial}{\partial t}\tilde{\rho}_{32} = i\left(\Delta_d + \frac{i\gamma_{32}}{2}\right)\tilde{\rho}_{32} + \left\{i\Omega_d(\tilde{\rho}_{33} - \tilde{\rho}_{22}) - i\Omega_p\tilde{\rho}_{31} + i\Omega_c{}^*\tilde{\rho}_{12}\right\}, \tag{8}$$

$$\tilde{\rho}_{11} + \tilde{\rho}_{22} + \tilde{\rho}_{33} = 1, \text{ and } \tilde{\rho}_{ij} = \tilde{\rho}_{ji}, (i,j = 1,2,3), \tag{9a, 9b}$$

Within these equations, the term Δ_p $(= \omega_p - \omega_{21})$ signifies the frequency detuning of the probe field relative to its corresponding transition, while Δ_d $(= \omega_d - \omega_{32})$, Δ_c $(= \omega_c - \omega_{31})$ denote the frequency detunings of the first and second control fields, respectively. In addition, total decay rates

of the respective states is denoted by γ_{ij}. Under the condition of weak probe approximation ($\Omega_p \ll \Omega_d, \Omega_c$), and satisfying the adiabatic condition, the solutions for ρ_{ij} from equations (3) to (8) are derived to the first order of Ω_p as, $\tilde{\rho}_{21}^{(1)} = \Omega_p \frac{D_p(0)}{D(0)}$, and $\tilde{\rho}_{31}^{(1)} = \Omega_p \frac{D_{p1}(0)}{D(0)}$. where, the term $D_p(0) = \left[\left(\Delta_p + \frac{i\gamma_{21}}{2}\right)\right]$, $D(0) = \left(\Delta_p + \Delta_c + i\frac{\gamma_{31}}{2}\right) * \left(\Delta_p + i\frac{\gamma_{21}}{2}\right) - |\Omega_d|^2$ and $D_{p1}(0) = \Omega_d$. With a polarization source term induced by the QD system is governed by-$P(\omega_p) = \varepsilon_0 \chi(\omega_p) E_p$, where $\chi(\omega_p)$ is the optical susceptibility, which can be written in the form of linear and nonlinear parts as follows: $\chi_p = \chi^{(1)} + \chi^{(3)}|E_p|^2 + \chi^{(5)}|E_p|^4$. We neglect the higher order terms of the susceptibilities at the probe frequency and casted as follows:

$$\chi^{(1)} = \frac{N|\mu_{12}|^2}{2\epsilon_0 \hbar \Omega_p} \tilde{\rho}_{12}^{(1)} = -\frac{N|\mu_{12}|^2}{2\epsilon_0 \hbar} \cdot \frac{D_p(0)}{D(0)}, \tag{10a}$$

$$\chi^{(3)} = -\frac{N|\mu_{12}|^2}{2\epsilon_0 \hbar \Omega_p} \tilde{\rho}_{12}^{(1)} \left(\left|\tilde{\rho}_{12}^{(1)}\right|^2 + \left|\tilde{\rho}_{13}^{(1)}\right|^2\right) = \frac{N|\mu_{12}|^4}{8\epsilon_0 \hbar^3} \cdot \frac{D_p(0)}{D(0)} \cdot \left\{\frac{|D_p(0)|^2 + |\Omega_c|^2}{|D(0)|^2}\right\}. \tag{10b}$$

$$\chi^{(5)} = \frac{N|\mu_{12}|^2}{2\epsilon_0 \hbar \Omega_p} \tilde{\rho}_{12}^{(1)} \left(\left|\tilde{\rho}_{12}^{(1)}\right|^2 + \left|\tilde{\rho}_{13}^{(1)}\right|^2\right)^2 = -\frac{N|\mu_{12}|^6}{32\epsilon_0 \hbar^5} \cdot \frac{D_p(0)}{D(0)} \cdot \left\{\frac{|D_p(0)|^2 + |\Omega_c|^2}{|D(0)|^2}\right\}^2, \tag{10c}$$

Now, we are poised to investigate the third and fifth-order nonlinear susceptibilities, considering various parameters associated with the GQD.

3. Results and Discussion

To proceed with the study, we have utilized the following system parameters: $N = 5 \times 10^{21} m^{-3}$, $\gamma_{21} = \gamma_{31} = 1.52 \times 10^{12} s^{-1}$, $\mu_{21} = 2.37 \times 10^{-28}\ C.m.$, $\omega_p = 1.935 \times 10^{14} s^{-1}$, $\Omega_p = 3.04 \times 10^{11} s^{-1}$, $\alpha = 9.71 \times 10^{16} m^{-1} s^{-1}$. To study the properties of the real and imaginary parts of the linear susceptibility, $Im\ \chi^{(1)}$ and $Re\ \chi^{(1)}$ profiles are shown as functions of normalized probe detuning (Δ_p/δ) by varing first-control Rabi frequencies (Ω_d/δ) in Figures 2(a) and 2(b), respectively. The numerical results in Fig. 2(a) indicate that for minimum values of the 1st-control Rabi frequency ($\Omega_d/\delta \simeq 0$), the probe field experiences significant absorption, displaying a sharp absorption peak at resonance $(\Delta_p/\delta = 0)$.As Ω_d/δ increases ($i.e., \Omega_d/\delta > 0$)the absorption peak is seen to split into two parts, indicating the EIT window formation, Here the normalizing term $\delta = 10^{11} s^{-1}$. The EIT window widens further on increasing Ω_d/δ. Fig.2 (b), indicates that, the dispersion profile given analytically by $Re\ \chi^{(1)}$ shows a negative slope around $\Delta_p/\delta = 0$ at initial value of $\Omega_d/\delta \simeq 0$. When control field $\Omega_d/\delta > 0$ is applied a dramatic change is observed in the behavior of $Re\ \chi^{(1)}$, it is observed that the slope of $Re\ \chi^{(1)}$transitions from negative to positive as Δ_p/δ shifts from negative to positive within the EIT window. This result suggests that by adjusting the control field Rabi frequency the dispersion regimes can be switched from 'anomalous' to 'normal'. Therefore, we can affirm that first-control Rabi frequency can regulate group-velocity of the probe field. Moving

forward, we examine the impact of the (Ω_c/δ) i.e. second-control field Rabi frequency on the dispersion and absorption profiles of the probe pulse in the GQD system, as shown in Figure 2(c). The profile of$Im\,\chi^{(1)}$ is depicted by varying the values of Ω_c/δ at a constant value of $\Omega_d/\delta\,(=5)$. The figure clearly shows that in the absence of the second-control field $\Omega_c/\delta = 0$, two side absorption peaks are observed at around the off-resonant positions $\Delta_p/\delta \approx \pm 5$ of the probe. These peaks are symmetric and have equal amplitudes.As the values of Ω_c/δ increase, the amplitude of the absorption peak at $\Delta_p/\delta \approx +5$ increases, while the amplitude at $\Delta_p/\delta \approx -5$ decreases. Meanwhile, Figure 2(d) shows the profile of $Re\,\chi^{(1)}$for different values of Ω_c/δat a constant $\Omega_d/\delta\,(=5)$. Therefore, we can establish that, the behavior of both the linear absorption and dispersion of the probe field can be manipulated as desired by adjusting the second-control Rabi frequency.

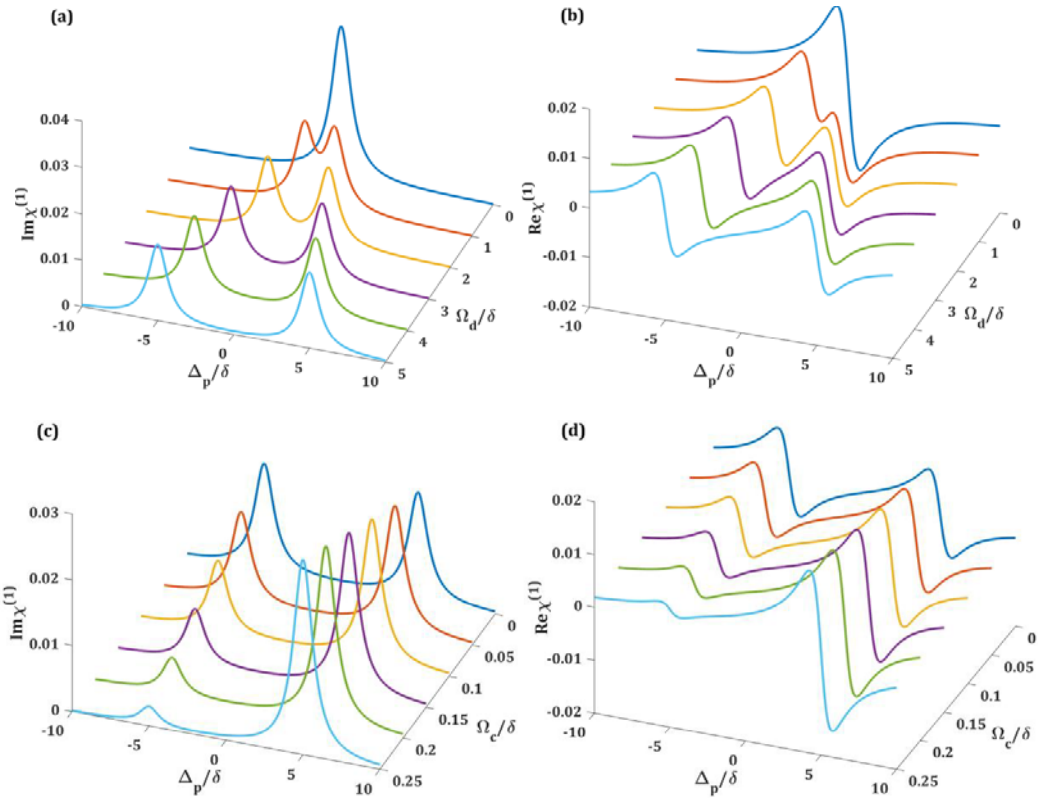

Fig.2: The variation of (a) $Im\chi^{(1)}$ and (b) $Re\chi^{(1)}$ with respect to Δ_p/δ for different values of Ω_d/δ. Next the variation of (c) $Im\chi^{(1)}$ and (d) $Re\chi^{(1)}$ with respect to Δ_p/δ for different values of Ω_c/δ.

In Fig. 3, we graphically present $Re\chi^{(3)}$, in the function of probe field detuning Δ_p/δ with the variation of two control field Rabi frequencies Ω_d/δ, and Ω_c/δ. In the Fig. 3(a), with the first control field Rabi frequency Ω_d/δ turned off, i.e. $\Omega_d/\delta = 0$, the $Re\chi^{(3)}$ exhibits a single peak around the probe field detuning $(\Delta_p/\delta = 0)$. Upon activating Ω_d/δ an additional peak emerges in the profile $Re\chi^{(3)}$.

Further increasing the value of Ω_d/δ, is increased, the separation between these peaks widens. A significant finding from the $Re\chi^{(3)}$plot reveals a substantial Kerr nonlinear susceptibility on the order of approximately~$10^{-15}(m/V)^2$. Meanwhile, from the Fig. 3 (b), when the second control field Rabi frequency Ω_c/δ is applied at fixed the value of $\Omega_d/\delta(=5)$, we observed the two separated peaks at the probe field detuning ($\Delta_p/\delta \cong \pm 5$), which on further increases the value Ω_c/δ, the negative probe side peaks are gradually disappear, while the positive side peaks increases their height.

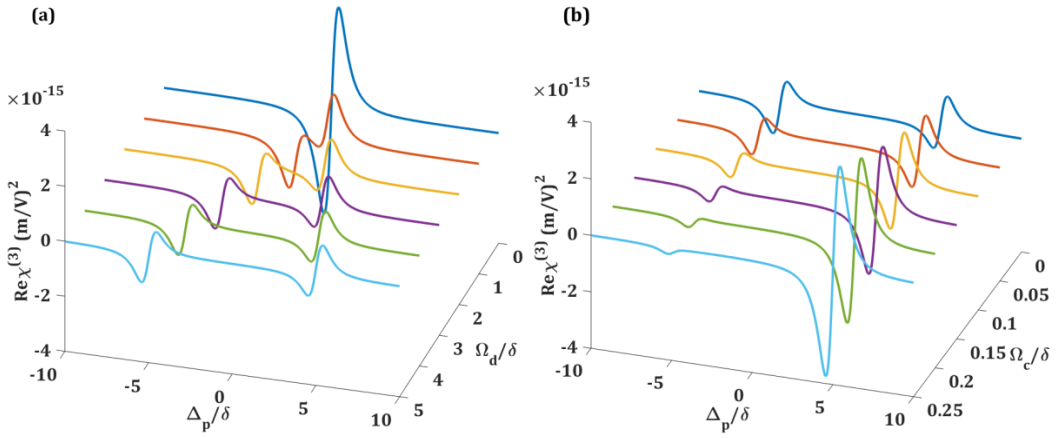

Fig.3: (a) Variation of the $Re\chi^{(3)}$ with respect to Δ_p/δ for the values of $\Omega_d/\delta = (0-5)$, (b) Variation of the $Re\chi^{(3)}$ with respect to Δ_p/δ for the values of $\Omega_c/\delta = (0-0.25)$.

Next, in Fig. 4(a), the real part of the fifth-order nonlinear susceptibility $Re\chi^{(5)}$is plotted, which a function of probe detuning (Δ_p/δ) under the effect of the first-control field (Ω_d/δ). As (Ω_d/δ) is varied from 0 to 5, the plot of $Re\chi^{(5)}$ reveals a notable enhancement in quintic nonlinearity within the transparency window, achieving magnitudes approximately on the order of ~$10^{-27}(m/V)^4$. We present Fig. 4(b), focusing on the fifth-order nonlinear susceptibility with the first control field Rabi frequency fixed at $\Omega_d/\delta = 5$, The figure illustrates that at $\Omega_c/\delta = 0$, there are two distinct peaks observed at the probe field detuning ($\Delta_p/\delta \cong \pm 5$). As the value of the second control field (Ω_c/δ) increases further, the peaks on the negative side gradually diminish, while the peaks on the positive side grow in height.

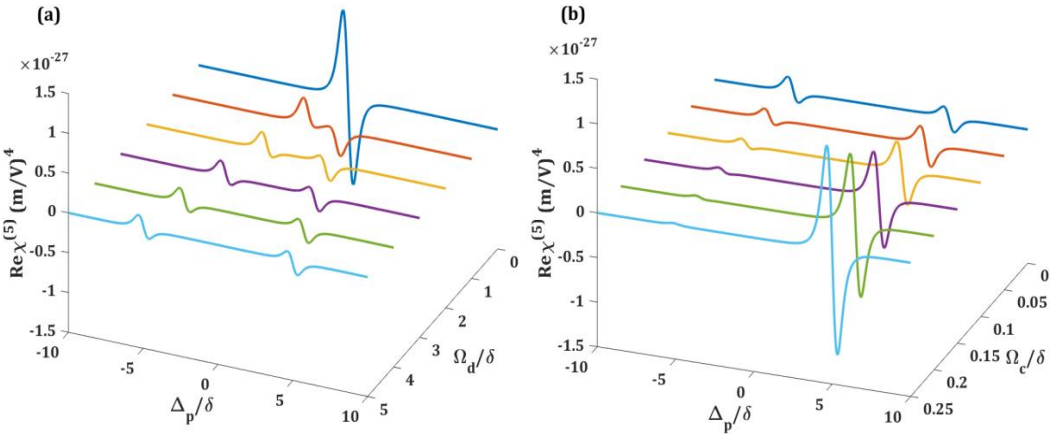

Fig.4: (a) Variation of the $Re\chi^{(5)}$ with respect to the ranging from $\Omega_d/\delta = (0-5)$, (b) Variation of the $Re\chi^{(5)}$ with respect to the ranging from $\Omega_c/\delta = (0-0.25)$.

At this juncture, it is worthwhile to compare the $\chi^{(3)}$and $\chi^{(5)}$ values identified in various materials with those observed in the graphene quantum dot utilized in this study, as detailed in Table 1. Table 1 clearly demonstrates that the $\chi^{(3)}$ and $\chi^{(5)}$ values identified in the present GQD system is significantly much larger than those reported for other materials.

Table 1: Comparison of $\chi^{(3)}$and $\chi^{(5)}$ values of different materials

Sl.No.	**Materials Type**	$\chi^{(3)}(m/V)^2$	$\chi^{(5)}(m/V)^2$	$(\lambda_p\ \mu m)$	**Ref.s**
1	As_2Se_3 glass	4.7×10^{-23}	-1.29×10^{-39}	1.064	19
2	SiO_2 fiber	4.2×10^{-23}	-4.2×10^{-38}	1.550	20
3	Semiconductor doped glass fiber	4.5×10^{-19}	1.6×10^{-34}	0.740	21
4	GaN/AlN Quantum Well	2.2×10^{-16}	NA	1.550	22
5	Graphene Quantum Dot	$\sim 1 \times 10^{-15}$	$\sim 1 \times 10^{-27}$	1.550	Present Paper

4. Conclusion

To conclude, in this theoretical investigation, we explore the behavior of linear and nonlinear susceptibilities in grapheme quantum dots, under the influence of electromagnetically induced transparency. We adopt a three-level, ladder type grapheme quantum dot system where a probe pulse interacts with the system to investigate nonlinear susceptibilities. By employing the density matrix approximation, we derive expressions for the first, third and fifth-order susceptibilities. Adjusting the control field Rabi frequencies, that allows us to manage the magnitude of linear and nonlinear susceptibilities induced by the probe field. Remarkably, we identify the third-order susceptibility on the order of $\sim 10^{-15}(m/V)^2$ and fifth order$\sim 10^{-27}(m/V)^4$. This work sheds light on the intricate

interplay between nonlinearities, dispersions, and control parameters, with potential applications in nonlinear fields.

Acknowledgements: Authors thank Shri M. Hoque, Hon'ble Chancellor of USTM for his immense support.

References

1. Niu, Y., Gong, S., Li, R., Xu, Z., & Liang, X., 2005, *Optics letters*, *30*(24), 3371-3373.
2. Hang, C., & Huang, G., 2010, *Optics Express*, *18*(3), 2952-2966.
3. Sun, H., Gong, S., Niu, Y., Jin, S., Li, R., & Xu, Z., 2006,*Physical Review B*, *74*(15), 155314.
4. Konar, S., Jana, S., & Mishra, M. 2005,*Optics Communications*, *255*(1-3), 114-129.
5. Agrawal, G. P., 2000, Nonlinear fiber optics. In *Nonlinear Science at the Dawn of the 21st Century* (pp. 195-211). Berlin, Heidelberg: Springer Berlin Heidelberg.
6. Yang, W. X., & Lee, R. K., 2008, *Optics Express*, *16*(22), 17161-17170.
7. Luo, X. Q., Wang, D. L., Zhang, Z. Q., Ding, J. W., & Liu, W. M., 2011, *Physical Review A*, *84*(3), 033803.
8. Marangos, J.P., 1998. Electromagnetically induced transparency. *Journal of modern optics*, *45*(3), pp.471-503.
9. Borgohain, N., Belic, M. and Konar, S., 2015. Giant parabolic nonlinearities at infrared in Λ-type three level multiple quantum wells. *Annals of Physics*, *361*, pp.107-119
10. Borgohain, N. and Konar, S., 2016. The effects of control field detuning on the modulation instability in a three-level quantum well system. *Journal of Applied Physics*, *119*(21)
11. Zhang, Y., Wang, J., & Xu, Z. (2017). Enhanced Kerr nonlinearity in quantum dots under electromagnetically induced transparency. *Applied Physics Letters, 110*(19), 191103
12. Hachim, F.K., Al-Nashy, B.O. and Al-khursan, A.H., 2023. Slow light in a double quantum dot system. *Optical and Quantum Electronics*, *55*(9), p.831
13. Xu, X., & Malko, A. V. (2004). Large third-order nonlinear optical coefficients in semiconductor quantum dots. *Journal of Applied Physics, 95*(8), 3983-3987.
14. Klimov, V. I. (2010). Nanocrystal Quantum Dots: From Fundamental Photophysics to Multicolor Luminous Objects and Photonic Devices. *Annual Review of Physical Chemistry, 58*, 635-673
15. Liu, C., Shen, Y., & Zhang, T. (2019). Investigating quintic nonlinearity in quantum dot systems under EIT. *Optical Materials Express, 9*(12), 4842-4851
16. Kang, M. S., Lee, K. H., & Kim, S. W. (2013). Observation of substantial quintic nonlinearity in semiconductor quantum dots. *Optics Letters, 38*(14), 2612-2615
17. Chen, W., Bao, J., & Xia, Y. (2016). Fifth-order nonlinear optical processes in quantum dot systems. *Physical Review B, 94*(4), 045201
18. Sahrai, M., & Abbasabadi, M., 2018, *Applied Optics*, *57*(3), 521-526
19. Boudebs, G., Cherukulappurath, S., Leblond, H., Troles, J., Smektala, F.,& Sanchez, F., 2003, *Optics Communications*, *219*(1-6), 427-433.
20. Pushkarov, D., &Tanev, S., 1996, *Optics Communications*, *124*(3-4), 354-364.
21. Schmid, W., Vogtmann, T., &Schwoerer, M., 1995, *Optics communications*, *121*(1-3), 55-62.
22. Hamazaki, J., Matsui, S., Kunugita, H., Ema, K., Kanazawa, H., Tachibana, T., ...&Kishino, K., 2004, *Applied physics letters*, *84*(7), 1102-1104.